The effects of shear on delamination in layered materials

S. Li[1], J. Wang[1] and M. D. Thouless[1,2]

[1]*Department of Mechanical Engineering*
[2]*Department of Materials Science & Engineering*
University of Michigan
Ann Arbor, MI 48109, U.S.A.

Keywords: *adhesion and adhesive (A), delamination (A), energy-release rate (A), fracture (A), elastic material (B)*

Abstract

The effect of transverse shear on delamination in layered, isotropic, linear-elastic materials has been determined. In contrast to the effects of an axial load or a bending moment on the energy-release rate for delamination, the effects of shear depend on the details of the deformation in the crack-tip region. It therefore does not appear to be possible to deduce rigorous expressions for the shear component of the energy-release rate based on steady-state energy arguments or on any type of modified beam theory. The expressions for the shear component of the energy-release rate presented in this work have been obtained using finite-element approaches. By combining these results with earlier expressions for the bending-moment and axial-force components of the energy-release rates, the framework for analyzing delamination in this type of geometry has been extended to the completely general case of any arbitrary loading. The relationship between the effects of shear and other fracture phenomena such as crack-tip rotations, elastic foundations and cohesive zones are discussed in the final sections of this paper.

(March 2003)

1. Introduction

Linear-elastic fracture mechanics expressions for the delamination of layered materials subjected to bending and axial loading (Fig. 1) were derived by Suo and Hutchinson (Suo and Hutchinson, 1990; Hutchinson and Suo, 1992). The magnitude of the energy-release rate, $\mathcal{G}_M$, and the complex stress-intensity factor, K_M, associated with a bending moment, M, are given by (Suo and Hutchinson, 1990)

$$\sqrt{\bar{E}_1 \mathcal{G}_M} = f_M(\alpha, H) M h_1^{-3/2} = \sqrt{\left(1-\beta^2\right)/\left(1-\alpha\right)}\left|K_M\right| \qquad (1a)$$

where $\bar{E} = E/\left(1-\nu^2\right)$ in plane strain or $\bar{E} = E$ in plane stress, E is Young's modulus, ν is Poisson's ratio, and the subscripts 1 and 2 denote arms 1 and 2 (Fig. 1). The first Dundurs parameter, α, is given by $\alpha = (\Sigma\text{-}1)/(\Sigma\text{+}1)$, where $\Sigma = \bar{E}_1/\bar{E}_2$. The second Dundurs parameter, β, is given by

$$\beta = \frac{\Sigma f(\nu_2) - f(\nu_1)}{\Sigma + 1}$$

and $$f(\nu) = \frac{1-\nu}{2}$$ in plane stress

or $$f(\nu) = \frac{1-2\nu}{2(1-\nu)}$$ in plane strain.

h is the depth of the arms, $H = h_1/h_2$, and the constant $f_M(\alpha, H)$ is given by

$$f_M(\alpha, H) = \left\{6\left[1+\left(\frac{1+\alpha}{1-\alpha}\right)H^3\right]\right\}^{1/2}. \qquad (1b)$$

The magnitude of the energy-release rate, $\mathcal{G}_P$, and the complex stress-intensity factor, K_P, associated with an axial load, P, (when the bending moment, M, is equal to zero) is given by (Suo and Hutchinson, 1990)

$$\sqrt{\bar{E}_1 \mathcal{G}_P} = f_P(\alpha, H) P h_1^{-1/2} = \sqrt{\left(1-\beta^2\right)/(1-\alpha)}\left|K_P\right| \qquad (2a)$$

where,

$$f_P(\alpha, H) = \left[0.5 + \left(\frac{1+\alpha}{1-\alpha}\right)\left(1.5H^3 + 3H^2 + 2H\right)\right]^{1/2}. \qquad (2b)$$

Energy-release rates for arbitrary combinations of bending moments and axial loads can be determined by adding the individual components of the stress-intensity factors in a vectorial fashion, provided the appropriate phase angles for pure bending, ψ_M, and axial loading, ψ_P, are known (Fig. 2). These phase angles are generally defined so that they are zero when the imaginary part of the quantity $Kh_1^{i\varepsilon}$ is zero (Suo and Hutchinson, 1990), where

$$\varepsilon = \frac{1}{2\pi} \ln \frac{1-\beta}{1+\beta}, \qquad (3)$$

From Fig. 2 it can be seen that the energy-release rate for combined loading is given by

$$\mathcal{G} = \mathcal{G}_P + \mathcal{G}_M + 2\left(\mathcal{G}_P \mathcal{G}_M\right)^{1/2} \cos\gamma_{PM} \quad , \qquad (4a)$$

or,

$$\bar{E}_1 \mathcal{G} = f_P^2(\alpha, H)\frac{P^2}{h_1} + f_M^2(\alpha, H)\frac{M^2}{h_1^3} + 2 f_P(\alpha, H) f_M(\alpha, H)\frac{PM}{h_1^2}\cos\gamma_{PM} \ , \qquad (4b)$$

where $f_M(\alpha, H)$ and $f_P(\alpha, H)$ are given by Eqn. (1) and (2), and

$$\begin{aligned} \gamma_{PM} &= \psi_P - \psi_M \\ &= \cos^{-1}\left\{\frac{(1+\alpha)}{(1-\alpha)}\frac{3H^2}{f_M(\alpha, H) f_P(\alpha, H)}\right\}. \end{aligned} \qquad (5)$$

If the phase angle for one of the two loading conditions is known, the other can be immediately calculated from Eqn. 5. The two phase angles are functions of α,

β and H. They were calculated by Suo and Hutchinson (1990), and the full results can be found in that reference. Examples of $\psi_M(\alpha, 0, H)$ for the special case of $\beta = 0$ are reproduced in Table 1[1], since they are used in the present paper.

These results of Suo and Hutchinson (1990) allow the interfacial fracture mechanics of any general bi-layer geometry to be calculated when only bending moments and axial loads act at the crack tip. However, in general, there will be a transverse shear force, V, at the crack tip in addition to a bending moment and an axial force (Fig. 3). The contribution of this transverse shear force to the energy-release rate needs to be incorporated in a full analysis of the interfacial fracture mechanics of bi-layers. One well-known example where this transverse shear force is significant is the double-cantilever beam (D.C.B.) geometry in which the moment is supplied to the crack tip by the action of a remote load. Indeed, it has been noted by a large number of authors that there is an additional contribution to the energy-release rate (Gillis and Gilman, 1964,; Mostovoy *et al.*, 1967; Wiederhorn *et al.*, 1968; Kanninen, 1973, 1974; Suo *et al.*, 1991; Bao *et al.*, 1992; Sun and Pandey, 1994; Williams, 1987, 1989, 1995), or to the stress-intensity factor (Fichter, 1983), beyond that expected only from pure bending. Previous explanations for this correction have included both the effects of shear, and "root-rotation" or other manifestations of elastic deformation ahead of the crack tip. It will be shown in this paper that while the correction can be completely and accurately accounted for in terms of the shear component of the energy-

[1] The values presented in Table 1 have been recalculated by the present authors using finite-element techniques. These represent some additional values of H, and some of the values appear to be slightly more accurate than the original values given in Suo and Hutchinson (1990).

release rate, crack-tip deformation does affects this component in a way that it does not affect the other two components.

The major thrust of this paper is to determine the effects of transverse shear on the energy-release rate and phase angle for delamination. When combined with the results of Suo and Hutchinson (1990), this analysis completes the general solution for plane, linear-elastic, interfacial fracture mechanics of layered materials. By incorporating crack-tip shear, bending and axial loading, these results can be used to calculate energy-release rates and phase angles for any beam-like geometry subjected to arbitrary loading. As particular examples, it is shown that this approach provides complete descriptions for the mechanics of various double-cantilever beam geometries that are in excellent agreement with finite-element calculations. Furthermore, the results also allow an understanding to be developed for the relative roles of shear, cohesive zones, root-rotation, and elastic foundations on the fracture behavior of layered materials.

2. Calculations and results

The energy-release rate associated with a moment, M, at the crack tip can be computed from a geometry in which the arms are subjected to a pure bending moment (Fig. 1), while the energy-release rate associated with an axial load, P, at the crack tip can be computed from a geometry in which the arms are subjected to a uniform load plus the required compensating moment (Fig. 1). The effect of a transverse shear force, V, acting at the crack tip can be determined by examining a geometry in which the moment at the crack tip resulting from an applied shear force is exactly cancelled by a pure moment of equal and opposite

magnitude (Fig. 4a). It should be noted that while a crack parallel to the axis of a beam does not affect the stress distribution caused by an axial load or a bending moment (Suo and Hutchinson, 1990), it does affect the stress distribution caused by a shear force. Therefore, for completeness, the results presented in this paper include the effects of a single transverse shear force acting on only one arm (Fig. 4b), in addition to the effects of equal forces acting on both arms (Fig. 4a).

The analysis was performed numerically using the ABAQUS (version 5.8) finite-element code. The crack tip was surrounded by a square mesh of 30 rings each of which contained 160 eight-noded, isoparametric, plain-strain elements. The two modes of energy-release rate were determined using the virtual-crack extension method (Parks, 1974; Haber and Koh, 1985; Matos *et al.*, 1989). To ensure an acceptable level of accuracy, the mesh sensitivity and effects of remote boundary conditions were explored, and estimates of the levels of uncertainty are included in the tables of results presented in this paper. The shear forces were applied as point loads at the centroidal axes of the beams.

A series of systematic, parametric calculations showed that, provided the crack is long enough, the phase angles and energy-release rates are independent of the crack length, a. Generally, these crack-length independent results are realized when the distance to the end of either beam is greater than its thickness. The magnitudes of the energy-release rates, $\mathcal{G}_V$ and $\mathcal{G}_{V_1}$, and the complex stress-intensity factors, K_V and K_{V_1}, associated with pure shear forces acting at the crack tip are given by

$$\sqrt{\bar{E}_1 \mathcal{G}_V} = f_V(\alpha, \beta, H) V h_1^{-1/2} = \sqrt{(1-\beta^2)/(1-\alpha)}\,|K_V|, \qquad (6a)$$

for a double-shear force (Fig. 4a), and

$$\sqrt{\bar{E}_1 \mathsf{G}_{V_1}} = f_{V_1}(\alpha,\beta,H) V h_1^{-1/2} = \sqrt{\left(1-\beta^2\right)/(1-\alpha)}\left|K_{V_1}\right|, \qquad (6b)$$

for a single shear force (Fig. 4b). The phase angles are of the form $\psi_V(\alpha,\beta,H)$ and $\psi_{V_1}(\alpha,\beta,H)$._ While these equations are very similar in form to Eqns. 1 and 2, analytical results do not exist for $f_V(\alpha, \beta, H)$ and $f_{V_1}(\alpha,\beta,H)$; they have to be found numerically. These numerical solutions indicate that the second Dundurs parameter, β, not only affects the phase angle, but also has a very small influence on the magnitude of the energy-release rate. This is in contrast to the solutions for an axial load or bending moment where β affects only the phase angle. Sets of values for $f_V(\alpha, 0, H)$, $f_{V_1}(\alpha,\beta,H)$, $\psi_V(\alpha, 0, H)$, and $\psi_{V_1}(\alpha,\beta,H)$ are given in Tables 2 and 3 for a full range of H, and for different values of the modulus mismatch (with $\beta = 0$).

3. Discussion

3.1 General beam-like geometries

The energy-release rate and phase angle for a layered material subjected to an arbitrary combination of axial load, P, transverse load, V and bending moment, M at the crack tip (Fig. 3) can now be calculated. The energy-release rate is given by

$$\begin{aligned}\bar{E}_1 \mathsf{G} = {} & f_P^2(\alpha,H)\frac{P^2}{h_1}\left[1+2\left(\frac{f_M(\alpha,H)}{f_P(\alpha,H)}\right)\left(\frac{M}{Ph_1}\right)\cos\gamma_{PM}+2\left(\frac{f_V(\alpha,H)}{f_P(\alpha,H)}\right)\left(\frac{V}{P}\right)\cos\gamma_{PV}\right] \\ & + f_M^2(\alpha,H)\frac{M^2}{h_1^3}\left[1+\left(\frac{f_V(\alpha,\beta,H)}{f_M(\alpha,H)}\right)^2\left(\frac{Vh_1}{M}\right)^2+2\left(\frac{f_V(\alpha,\beta,H)}{f_M(\alpha,H)}\right)\left(\frac{Vh_1}{M}\right)\cos\gamma_{MV}\right]\end{aligned} \qquad (7)$$

where, $\gamma_{PM} = \psi_P(\alpha,\beta,H) - \psi_M(\alpha,\beta,H)$

$\gamma_{PV} = \psi_P(\alpha,\beta,H) - \psi_V(\alpha,\beta,H)$

$\gamma_{MV} = \psi_M(\alpha,\beta,H) - \psi_V(\alpha,\beta,H).$

The phase angle is given by

$$\psi = \tan^{-1}\left\{\frac{f_M(\alpha,H)\sin\psi_M + f_P(\alpha,H)\{Ph_1/M\}\sin\psi_P + f_V(\alpha,\beta,H)\{Vh_1/M\}\sin\psi_V}{f_M(\alpha,H)\cos\psi_M + f_P(\alpha,H)\{Ph_1/M\}\cos\psi_P + f_V(\alpha,\beta,H)\{Vh_1/M\}\cos\psi_V}\right\} \tag{8}$$

As an example, consider a double-cantilever beam with a crack length *a* that is loaded remotely by applied loads, *F*. The crack tip is subjected to transverse shear forces, $V = F$, bending moments, $M = Fa$, and no axial loads. Therefore, the energy-release rate can be obtained from Eqn. 7:

$$\bar{E}_1 G = f_M^2(\alpha,H)\frac{(Fa)^2}{h_1^3}\left\{1+\left(\frac{f_V(\alpha,0,H)}{f_M(\alpha,H)}\right)^2\left(\frac{h_1}{a}\right)^2 + 2\left(\frac{f_V(\alpha,0,H)}{f_M(\alpha,H)}\right)\left(\frac{h_1}{a}\right)\cos\gamma_{MV}\right\}, \tag{9}$$

and the phase angle can be obtained from Eqn. 8:

$$\psi = \tan^{-1}\left\{\frac{\{a/h_1\}f_M(\alpha,H)\sin\psi_M + f_V(\alpha,0,H)\sin\psi_V}{\{a/h_1\}f_M(\alpha,H)\cos\psi_M + f_V(\alpha,0,H)\cos\psi_V}\right\}, \tag{10}$$

where $f_M(\alpha, H)$ is given by Eqn. 1(b), and $\psi_M(\alpha, 0, H)$, $f_V(\alpha, 0, H)$ and $\psi_V(\alpha, 0, H)$ are given in Tables 1 and 2. In particular, if $\alpha = 0$ and the geometry is symmetrical so that $H = 1$ and $\psi_M = \psi_V = \gamma_{MV} = 0$, then $f_M(0, 1) = \sqrt{12}$ and $f_V(0, 0, 1) = 2.335$. Equation (9) then reduces to the simple form of

$$G = \frac{12(Fa)^2}{\bar{E}h^3}\left(1 + 0.674\frac{h}{a}\right)^2. \tag{11}$$

Apart from a minor correction in the third significant figure, this is indistinguishable from the empirical fit to finite-element calculations given by

Bao *et al.* (1992).[2] Further examples of comparisons between Eqns. 9 and 10 and the results of finite-element calculations for different values of α and H are given in Figs. 5 and 6. It will be seen that the concept of separating the energy-release rate into a moment component and a shear component provides an excellent method of analyzing these geometries. In particular, these results now allow the effect of modulus mismatch on the phase angle and energy-release rate to be determined for asymmetrical double-cantilever beams.

The concept of splitting the applied loads into a moment, an axial force and a shear force acting at the crack tip can be applied to many other geometries, even those exhibiting non-linear deformations.[3] For example, consider a symmetrical double-cantilever beam (D.C.B.) undergoing large-scale deformations, so that the lever arm between the applied load and the crack tip gets smaller as deformation proceeds. Eventually, the geometry changes from a D.C.B. configuration to a symmetrical 90º T-peel configuration. Therefore, the energy-release rate must vary between one limit given by Eqn. 11 that is valid for small deformations, and a second limit given by the T-peel result (Kendall, 1975) of $\mathcal{G}/Eh = (P/Eh)(1+P/Eh)$ that is valid for large deformations (provided the strains remain linear). Using a non-linear finite-element analysis to compute the lever arm and, hence, the crack-tip bending moment, Eqn. 9 was used to

[2] It should be noted that the ASTM standard (D3433-93) for tests using double-cantilever beams is based on the equation $\mathcal{G} = 4F^2(3a^2 + h^2)/\bar{E}h^3$, which comes from an approximate analytical result for the effects of shear as described by Mostovoy *et al.* (1967). This equation has an incorrect crack-length dependence and gives an error in $\mathcal{G}$ that can be as large as 52% for $a/h = 1$. The error is still as large as 12% for $a/h = 10$. These errors are only slightly less than those associated with not correcting for shear at all.

[3] It should be noted that warping of the beam occurs owing to the shear force and to the non-uniformity of the stresses at the crack tip region. This limits the accuracy of the analytical

calculate the energy-release rate. Finite-element methods were also used to calculate a numerical value for the energy-release rate. The excellent agreement between these two sets of results, and the transition between the two limiting solutions can be seen in Fig. 7. A final comment on calculating energy-release rates for geometries undergoing large deformations or rotations by means of the approach presented in this paper is to note that if the geometry of interest includes a crack-tip region that is subjected to a rigid-body rotation (such as would occur in a bending beam), and the direction of the applied load is fixed, care has to be taken to resolve the applied load into the appropriate shear and axial components acting at the crack tip before using Eqns. 7 and 8.

3.2 Comment on analytical approaches

The results of Eqns. 1 and 2 for the bending-moment and axial-load components of the energy-release rate can readily be obtained from simple beam theory. The similarity in form between these two equations and Eqn. 6 may suggest the possibility of developing a similar approach for the shear component using higher-order beam theories that incorporate shear. Unfortunately, this does not seem to be possible. A hint of the problem is provided by comparing the details of Eqns. 1(a) and 1(b), which can be obtained by beam theory, to Eqn. 6, which that cannot. The numerical constants in the first two equations depend only on the geometry and one Dundurs parameter, α. The numerical constant in Eqn. 6 has an additional dependence on the second Dundurs parameter, β. This difference indicates that while the bending-moment and axial-load components of the energy-release rate are unaffected by details of the

---

approach to problems involving relatively small strains (although large deformations can be

deformation in the crack tip region, the shear component is fundamentally affected by this local deformation.

The fact that the bending-moment and axial-load components of the energy-release rate are unaffected by details of the deformation in the crack-tip region manifests itself by the existence of solutions that can be obtained by steady-state energy-balance arguments. A similar steady-state argument cannot be developed for shear because a state of uniform shear cannot act over the length of a beam in the absence of an associated gradient in bending moment. Therefore, while Eqn. 6 correctly implies that a crack tip can be acted on by pure shear (any bending moment component from the applied shear load being eliminated by the application of an equal and opposite pure bending moment), it would be misleading to consider this equation to be a steady-state solution in the same way that Eqn. 2(a) can be considered to be a steady-state solution for loading by a pure bending moment. It can readily be shown that a steady-state energy balance based only on the parabolic shear-stress distribution that exists well away from the crack tip and the point of load application does not result in the correct result for the shear component of the energy-release rate. This is because such an approach neglects the contribution of the crack tip deformation on the energy-release rate.

The deformation in the crack-tip region has been described in terms of "root-rotation" effects, where planes rotate in response to the applied loading (Williams, 1987; 1989), and "elastic-foundation" effects, where there are strains perpendicular to the crack plane (Kanninen, 1973, 1974). These effects are

---

accommodated).

discussed in more detail in subsequent sections. This deformation in the crack-tip region occurs to various degrees when any shear force, bending moment or axial load is applied to a beam-like geometry. However, it only affects the shear component of the energy-release rate. When calculating the moment and axial-load components of the energy-release rate, it doesn't matter what assumption is made about the boundary conditions where the beam is attached to the substrate at the crack tip; any assumption results in rigorously correct solutions because the crack-tip deformation doesn't contribute to the solution. Conversely, since the crack tip region does affect the shear component of the energy-release rate, the results of beam-based analyses are dependent on the nature of the assumptions made about the boundary conditions at the crack tip. Rigorous solutions for the shear component of the energy-release rate can only be obtained by an analysis of the full elastic problem including a correct description of the interface between the two arms. This is the analysis that has been performed in the present paper by means of a finite-element method.

3.3 Root rotations

Consider a section just behind the crack tip that is initially normal to the centroidal axis of an arm in a beam-like geometry. After loading, this section may rotate as shown in Fig. 8. Two types of rotation can occur. The angle between the section and the centroidal axis can change – this is the shear strain at the crack tip. The other type of rotation occurs when the centroidal axis and the section rotate together – this is "root rotation." In general, the magnitude of root rotation will not be uniform across the section, but the average value is

considered to be the "root rotation angle" in this paper. If the crack length is long enough to avoid boundary effects, the root rotation angle is given by

$$\theta_o = c_M \frac{M}{\bar{E}_1 h_1^2} + c_P \frac{P}{\bar{E}_1 h_1} + c_V \frac{V}{\bar{E}_1 h_1}, \tag{12}$$

where c_M, c_P, c_V are functions of the elastic constants and geometry. The first two coefficients, c_M and c_P, appear to be functions of α and β, whereas c_V appears to be a function of all three non-dimensional elastic constants. Values for all three coefficients are given in Fig. 9 as a function of α (with $\beta = 0$).[4]

Root rotation is sometimes invoked as a reason for the difference between the expressions for the energy-release rate of a layered material loaded by a moment and the same geometry loaded by an applied force. However, it can be seen from Eqn. 12 that root rotation is a very general effect, and is not associated just with the application of a shear force. Furthermore, the general expressions of Eqns. 1, 2 and 7 for the components of the energy-release rate are always valid and completely incorporate any possible effects of root rotation. Therefore, root rotation should not be considered as an independent contributor to the energy-release rate. Energy-release rates can be calculated with reference only to the crack-tip axial load, moment and shear force; root rotation does not provide an independent contribution. However, root rotation can play a very important role in the fracture mechanics of beam-like geometries if it causes a large enough change in geometry to affect significantly the calculation of the crack-tip forces and moments for a particular geometry. For example, the original calculations (Hutchinson and Suo, 1992) for the energy-release rate of buckling-driven

delaminations under compressively-stressed thin films were based on the assumption of "clamped boundary conditions." It was assumed that the critical stress required to buckle a film with a given size of delamination is identical to that of a plate of the same size, but clamped around the perimeter. The energy-release rate was then calculated from Eqns. 1 and 2 by determining the bending moment and axial force that act at the clamped boundaries of a buckled plate. A clamped boundary is tantamount to assuming no root rotation at the crack tip. However, as shown by Cotterell and Chen (2000), and Yu and Hutchinson (2002), this assumption of a clamped boundary (no root rotation) may cause significant errors in calculating the crack-tip moment and force if the substrate is compliant. Under these conditions, accurate calculations of the moment and force need to incorporate the root rotation. Once these have been calculated, Eqns. 1 and 2 then provide rigorous solutions for the energy-release rate.

Shear does not contribute to the energy-release rate in these buckling-driven delamination problems. However, it does contribute to other significant thin-film geometries such as the blister test and the peel test. Existing analyses of the blister test are based on the assumption of a clamped boundary at the crack tip, and they neglect the effects of shear (Jensen, 1991; Jensen and Thouless, 1993). While the energy-release rate for an elastic peel test can be obtained directly from a steady-state energy-balance argument (Kendall, 1975), existing calculations of the phase angle also ignore the effects of shear (Thouless and Jensen, 1992). Shear effects in a peel test exhibiting plastic deformation have

[4] Note that in the results presented in Fig. 9, the root rotation is defined as the average rotation of the plane at the crack tip. This is a different definition from that used by Yu and Hutchinson (2002) and is responsible for the slight discrepancy between the two sets of results.

been identified (Yang et al., 2001), as have shear effects in wedge tests with plastic deformation (Yang *et al.*, 1999).

3.4 Cohesive zones

Cohesive zones and elastic foundations are two inter-related concepts that also appear in the literature in connection with the effects of shear. The final two sections of the discussion will attempt to clarify the role of these two phenomena in the elastic fracture mechanics of layered materials. The discussion so far has been limited to problems with uniform linear-elastic constitutive properties throughout both portions of a bi-material beam. If the cohesive tractions at the interface contribute negligibly to the overall compliance of the system, this discussion is valid, and linear-elastic fracture mechanics is appropriate. However, additional complications arise if the cohesive tractions between the two materials contribute significantly to the compliance of the system.

It has been demonstrated (Tvergaard and Hutchinson, 1992) that there are two important cohesive parameters that dominate mode-I fracture: the cohesive strength, $\hat{\sigma}$, and the toughness, Γ_{Io}. Details of the shape of the traction-separation law for the cohesive tractions have a minor influence on the mechanics. Using a cohesive-zone model described elsewhere (with a trapezoidal traction-separation law) (Yang *et al.*, 1999; Cavalli and Thouless, 2001), the effects of these two dominant parameters can be explored using a symmetrical, linear-elastic, double-cantilever beam as a model. The resultant load-displacement curves are shown in Fig. 10, and compared to the results of linear-elastic calculations. These curves show that if $\bar{E}\Gamma_{Io}/\hat{\sigma}^2 h$ is less than about 0.4, the cohesive strength has a negligible effect on the deformation and fracture

of the beam, and the toughness is the only interfacial parameter that affects fracture. The linear-elastic result of Eqn. 11, which incorporates shear, then provides an accurate description of the fracture mechanics, and the interfacial toughness can be obtained from a double-cantilever geometry by substituting the maximum load obtained experimentally into Eqn. 11 and equating the energy-release rate to the toughness.[5] The toughness of the interface is then the only interfacial parameter that affects fracture. If $\bar{E}\Gamma_{Io}/\sigma^2 h$ is greater than about 0.4, the peak load is significantly reduced from what would be predicted by L.E.F.M., and this approach would not be valid. Both the strength and compliance of the joint would then be required to find the fracture parameters (Suo *et al.*, 1992; Spearing and Evans, 1992).

Inspection of Fig. 10 suggests a simple, elegant and very practical way of deducing the interfacial toughness from a double-cantilever beam experiment when $\bar{E}\Gamma_{Io}/\sigma^2 h$ is unknown. It will be noted that the cohesive zone is fully developed at the peak load and, subsequently, the crack grows maintaining a cohesive zone of constant size ahead of its tip. In this regime the load-displacement plot does not depend on the cohesive strength. In other words, the LEFM results provide a master curve for crack propagation. (The results for different cohesive strengths are simply translated to different effective crack lengths.) It can be shown that this master curve relating the cracking load, F_c, to the crack-mouth opening displacement, δ, is given by

[5] It is noted that the standard formulation for the validity of linear-elastic fracture mechanics (L.E.F.M.) is that $h > 2.5\left(K_c/\sigma_Y\right)^2$, where σ_Y is the yield strength, and K_c is the fracture toughness of the interface. Recognizing that $K_c = \sqrt{\bar{E}\Gamma_{Io}}$, it can be seen that this standard formulation is

$$\left(\frac{F_c}{\bar{E}h}\right)^2 = \frac{1}{3\sqrt{3}}\left(\frac{\Gamma_{Io}}{\bar{E}h}\right)^{3/2}\left(\frac{\delta}{h}\right)^{-1}. \qquad (13)$$

Hence, if the experimental load and displacement are measured in this regime, Γ_{Io} can be determined directly from Eqn. (13) without any knowledge of the crack length or of the cohesive strength. Only the elastic properties and the thickness of the arms need to be known. This provides a powerful technique for analyzing symmetrical double-cantilever geometries even under L.E.F.M. conditions. Once the toughness has been obtained by this approach then, if $\bar{E}\Gamma_{Io}/\sigma^2 h > 0.4$, the cohesive strength can be found using a cohesive-zone model and comparing the predictions for the peak load (or / and the loading compliance) to the experimental observations.

3.5 Elastic-foundation models

An excellent solution for the energy-release rate of a double-cantilever beam can be found using elastic-foundation models (Kanninen, 1973, 1974; Williams, 1989, 1995; Williams and Hadavinia, 2002). The concept underpinning these analyses is that local deformation of the material immediately ahead of the crack tip affects the compliance of the system and influences the energy-release rate. This effect is incorporated in the analysis by assuming that, as shown in Fig. 11, the material between the mid-plane of the D.C.B. and the centroidal axis of an arm can be modeled as a Winkler elastic foundation bonded to a rigid surface (the plane of symmetry). The analysis essentially proceeds by considering a semi-infinite beam of elastic stiffness $\bar{E}h^3/12$ (per unit width) supported on an elastic foundation of stiffness k (per unit width) and loaded by a

essentially identical to the result indicated here with the cohesive strength of the interface being

moment M (per unit width) and a shear force V (per unit width) at one end. The displacement at the edge of the elastic foundation is given by (Barber, 2001)

$$u_o = \frac{2\lambda}{k} V + \frac{2\lambda^2}{k} M \ , \tag{14}$$

where $\lambda = \left(3k / \bar{E} h^3\right)^{1/4}$. Recognizing that there two halves to this mode-I geometry, the energy-release rate for the crack can be written as

$$\mathsf{G} = k u_o^2 . \tag{15}$$

Hence, from Eqn. 14 it can be seen that

$$\bar{E}\mathsf{G} = \left[2.632 \left(\frac{\bar{E}}{hk} \right)^{1/4} \frac{V}{h^{1/2}} + \sqrt{12} \frac{M}{h^{3/2}} \right]^2 . \tag{16}$$

It is noted that the stiffness of the foundation has no effect on the moment component of the energy-release rate, and Eqn. 16 reduces to Eqn. 1 for $H = 1$ and $\alpha = 0$ if there is no shear force. However, the shear component of the energy-release rate is sensitive to assumptions about the stiffness of the foundation. This further emphasizes the point made in Section 3.2 that, while the moment component of the energy-release rate does not depend on the deformation in the crack-tip region, the shear component does.

A physical argument was made in Kanninen (1973) that $k \approx 2\bar{E} / h$. This results in a very good agreement with numerical results for the double-cantilever beam. However, it is interesting to note that if one chooses $k = 1.615\bar{E}/h$, Eqn. 16 becomes

$$\bar{E}\mathsf{G} = \left[2.335 V h^{-1/2} + \sqrt{12} M h^{-3/2} \right]^2 \ , \tag{17}$$

---

represented by the yield stress.

which is identical to Eqn. 11. This exact match to the rigorous solution for the shear component of the energy-release rate only works for the perfectly symmetrical case when the phase angle is zero. However, the approach (with the same value for k) can be used to obtain an approximate analytical result for $f_v(\alpha, 0, H)$. If the analysis is repeated for a asymmetrical double-cantilever beam (assuming again that the foundation can be split into two portions corresponding to each arm), the following result is obtained:

$$f_v(\alpha,0,H) \approx 1.65\sqrt{1+\left(1+\alpha\right)\left(1-\alpha\right)^{-1}}\,H\,. \qquad (18)$$

It will be observed from Table 2(a) that this result generally provides quite a good fit to the values given in Table 2(a). An elastic foundation approach can also be used to provide a good approximation to the solution for the energy-release rate associated with a combined shear and bending moment (Williams, 1995). While this approach can correctly reproduce the first two terms of Eqn. 9, it does not accurately describe the interaction between the two components (the last term in Eqn. 9); nor does it provide any information about the phase angle.

An approximate analytical result for a cohesive zone in a double-cantilever beam geometry can be developed using the elastic-foundation model. It should be noted that the springs for such a model need to include two elements in series. The first element represents the deformation of the arms, and can be modeled by springs that have a spring constant of $k_d = 1.615\,\overline{E}/h$. The second element represents the cohesive zone. As noted by Williams and Hadavinia (2002), analytical models can be developed for cohesive-zone elements with different types of constitutive properties. Here, the cohesive zone is represented by linear-elastic elements, so that the spring constant is given by

$$k_c = \sigma^2 / \Gamma_{Io} \tag{19}$$

(since there are two halves to the D.C.B. geometry). The effective spring constant is then given by

$$k = \frac{k_d k_c}{k_d + k_c} = \frac{1.615\left(\bar{E}\Gamma_{Io} / \sigma^2 h\right)}{1 + 1.615\left(\bar{E}\Gamma_{Io} / \sigma^2 h^2\right)}\ , \tag{20}$$

and, from Eqn. 16, the expression for the energy-release rate of a point-loaded double-cantilever beam with a crack of length a becomes

$$\mathcal{G} = \frac{12F^2a^2}{\bar{E}h^3}\left[1 + 0.674\frac{h}{a}\left(1 + 1.62\frac{\bar{E}\Gamma_{Io}}{\sigma^2 h}\right)^{1/4}\right]^2. \tag{21}$$

An expression for the load at which crack growth occurs, F_c, is then given by equating $\mathcal{G}$ to Γ_{Io}:

$$\frac{F_c}{\bar{E}h} = \left(\frac{\Gamma_{Io}}{12\bar{E}h}\right)^{1/2}\left[\frac{a}{h} + 0.674\left(1 + 1.62\frac{\bar{E}\Gamma_{Io}}{\sigma^2 h}\right)^{1/4}\right]^{-1} \tag{22}$$

This result is in moderately good agreement with the predicted fracture loads shown in the numerical data of Fig. 10. However, there is some discrepancy associated with the different choices of the cohesive law used in the two calculations.[6]

4. Conclusions

The forces and moments acting on the tip of a crack in a layered material under any general plane loading can be described in terms of an axial compressive load, a bending moment and a transverse shear load. It is possible to express the energy-release rate and the phase angle in terms of three separate

components associated with each of the three types of loading. In this paper, the results for the shear component have been presented. In contrast to the results for the moment and axial-force components, the shear component of the energy-release rate cannot be derived from either a steady-state energy argument or from a beam analysis (even a higher-order theory that incorporates shear). This is because the details of the crack-tip deformation play a crucial role in the case of shear. The effect of shear is not merely a second-order correction to a simple Euler-Bernoulli beam-theory approach to the mechanics of layered materials. Shear loading at the crack tip is an important and independent phenomenon that completes the triad of possible crack-tip loading configurations for a layered material. For example, in a short double-cantilever beam, the shear component can contribute as much as two thirds of the total energy-release rate. It is theoretically possible for the shear component to be even more dominant if, for example, a gradient of internal residual stresses in a thin film counteracts any moment associated with an applied load (as in Fig. 4).

The results presented in this paper for the shear component of the energy-release rate can be combined with the results previously derived by Suo and Hutchinson (1990) for the axial-load and bending-moment components to analyze any general loading of layered materials and other beam-like geometries. For example, it is possible to use Eqns. 10 and 11 to calculate the energy-release rate and phase angle of any double-cantilever beam geometry with a modulus mismatch and different thicknesses of arms. It has been shown that predictions

[6] The nature of the relationship between the fracture load and the cohesive strength (Eqn. 22) indicates how estimates of F_c for given values of σ are not be very sensitive to the assumed cohesive law, but estimates of σ obtained from observations of F_c are much more sensitive.

from this type of analysis provide excellent agreement with numerical calculations. A particular illustration of this analysis is the fracture mechanics of a symmetrical double-cantilever beam. It has been shown that the analysis results in the commonly accepted equation for the energy-release rate of a D.C.B. that includes a "correction factor" to the equation that is derived from considerations of pure bending. This "correction factor" arises from the shear component to the energy-release rate, it does not arise from factors such as root rotation, cohesive zones or elastic foundations. The significance of these phenomena and models in the mechanics of layered materials have been discussed in the last section of this paper.

Acknowledgements

This work was partially supported by NSF Grant No. CMS9624452, and by the Department of Mechanical Engineering, University of Michigan.

References

ASTM D3433-93 “Standard test method for fracture strength in cleavage of adhesives in bonded joints,” *American Society for Testing and Materials* (1993).

Bao, G., Ho, S., Suo Z., and Fan, B., “The role of material orthotropy in fracture specimens for composites,” *Int. J. Solids Structures*, **29**, 1105-1116 (1992).

Barber, J. R., chapter 7 in *Intermediate Mechanics of Materials*, McGraw Hill, NY, (2001).

Cavalli, M. N., and Thouless, M. D., “The effect of damage nucleation on the toughness of an adhesive joint,” *J. Adhesion*, **76**, 75-92 (2001).

Cotterell B., and Chen, Z., “Buckling and cracking of thin films on compliant substrate under compression,” *Int. J. Fract.*, **104**, 169-179 (2000).

Fichter, W.B., “Stress intensity factor for the double cantilever beam,” *Int. J. Fract.*, **22**, 133-143 (1983).

Gillis, P. P., and Gilman, J. J., “Double-cantilever cleavage mode of crack propagation,” *J. Appl. Phys.*, **35**, 647-658 (1964).

Haber, R. B., and Koh, H. M., “Explicit expressions for energy release rates using virtual crack extensions,” *Int. J. For Numerical Methods in Engineering*, **21**, 301-315 (1985).

Hutchinson, J. W., and Suo, Z., “Mixed-mode cracking in layered materials,” *Advances in Applied Mechanics*, **29**, 64-187 (1992).

Jensen, H. M., “On the blister test for interface toughness measurement,” *Eng. Fract. Mechs.*, **40**, 475-486 (1991).

Jensen, H. M, and Thouless, M. D., “Effects of residual stresses in the blister test,” *Int. J. Solids Struct.*, **30**, 779-795 (1993).

Kanninen, M. F., “Augmented double cantilever beam model for studying crack propagation and arrest,” *Int. J. Fract.*, **9**, 83-92 (1973).

Kanninen, M. F., “Dynamic analysis of unstable crack propagation and arrest in the DCB test specimen,” *Int. J. Fract.*, **10**, 415-430 (1974).

Kendall, K., “Thin-film peeling – the elastic term,” *Journal of Applied Physics*, **8**, 1449-1452 (1975).

Matos, P. P. L., McMeeking, R. M., Charalambides, P. G., and Drory, M. D., “A method for calculating stress intensities in bimaterial fracture,” *Int. J. Fract.*, **40,** 235-254 (1989).

Mostovoy, S., Crosley, P. B., and Ripling, E. J., “Use of crack-line loaded specimens for measuring plane strain fracture toughness,” *J. Matls.*, **2**, 661-681 (1967).

Parks, D. M., “A stiffness derivative finite element technique for determination of crack tip stress intensity factors,” *Int. J. Fract.*, **10**, 487-501 (1974).

Spearing, S. M. and Evans, A. G., "The role of bridging fibers in the delamination of brittle matrix composites," *Acta Metall. Mater.*, **40**, 2191-2199 (1992).

Sun, C. T., and Pandey, R. K., "Improved method for calculating strain energy release rate based on beam theory," AIAA Journal, **32**, 184-189 (1994).

Suo, Z., and Hutchinson, J. W., "Interface crack between two elastic layers.," *Int. J. Fract.*, **43**, 1-18 (1990).

Suo, Z., Bao, G., Fan, B., and Wang, T. C., "Orthotropy rescaling and implications for fracture in composites," *Int. J. Solids and Structures*, **28**, 235-248 (1991).

Suo, Z., Bao, G., and Fan, B., "Delamination *R*-curve phenomena due to damage," *J. Mech. Phys. Solids*, **40**, 1-16 (1992).

Thouless, M. D., and Jensen, H. M., "Elastic fracture mechanics of the peel-test geometry," *J. Adhesion*, **38**, 185-197 (1992).

Tvergaard, V., and Hutchinson, J. W., "The relationship between crack growth resistance and fracture process parameters in elastic plastic solids," *J. Mech. and Phys. Solid*s, **40**, 1377-1397 (1992).

Wiederhorn, S. M., Shorb, A. M. and Moses, R. L., "Critical analysis of the theory of the double cantilever method of measuring fracture-surface energies," *J. Applied Phys.*, **39**, 1569-1572 (1968).

Williams, J. G., "Large displacement and end block effects in the 'DCB' interlaminar test in modes I and II," *Journal of Composite Materials*, **21**, 330-347 (1987).

Williams, J. G., "End corrections for orthotropic DCB specimens," *Composites Science and Technology*, **35**, 367-376 (1989).

Williams, J. G., “Fracture in adhesive joints-the beam on elastic foundation model” *Proceedings of ASME International Mechanical Congress & Expositions*, 1112-1117 (1995).

Williams, J. G., and Hadavinia, H., “Analytical solutions for cohesive zone models,” *J. Mechs. Phys. Solids*, 809-825 (2002).

Yang, Q. D., Thouless, M. D., and Ward, S. M. “Analysis of the symmetrical 90^0-peel test with extensive plastic deformation,” *J. Adhesion*, **72**, 115-132 (2000).

Yang, Q. D, Thouless, M. D., and Ward, S. M., “Numerical Simulations of Adhesively-Bonded Beams Failing with Extensive Plastic Deformation,” *J. Mech. Phys. Solids*, **47**, 1337-1353 (1999).

Yu, H. H. and Hutchinson, J. W., “Influence of substrate compliance on buckling delamination of thin films,” *Int. J. Fract.*, **113**, 39-55 (2002).

Table 1 The phase angle, $\psi_M(\alpha, \beta, H)$, for delamination of a bilayer subjected to a pure bending moment and $\beta = 0$. The uncertainty of these results is better than ± 0.1°.

	α	**-0.8**	**-0.6**	**-0.4**	**-0.2**	**0**	**0.2**	**0.4**	**0.6**	**0.8**
H										
0.0		-43.3°	-42.3°	-41.0°	-39.6°	-37.9°	-35.9°	-33.4°	-30.1°	-24.9°
0.2		-43.0°	-41.3°	-39.4°	-37.3°	-34.8°	-31.8°	-28.1°	-22.9°	-14.3°
0.4		-41.5°	-38.4°	-35.1°	-31.6°	-27.5°	-22.8°	-16.9°	-8.9°	+4.0°
0.6		-39.2°	-34.1°	-29.1°	-23.8°	-18.1°	-11.8°	-4.3°	+5.2°	+18.5°
0.8		-36.0°	-28.8°	-22.1°	-15.4°	-8.6°	-1.3°	+6.6°	+15.8°	+27.3°
1.0		-32.4°	-23.0°	-14.9°	-7.3°	0.0°	+7.3°	+14.9°	+23.0°	+32.4°

Table 2(a) The coefficient $f_V(\alpha,\beta,H)$ for delamination of a bilayer subjected to a double transverse shear loads and $\beta = 0$. The uncertainties are ± 0.007 for $H \geq 0.2$.

	α	-0.8	-0.6	-0.4	-0.2	0	0.2	0.4	0.6	0.8
H										
0.0		see Table 3(a)								
0.2		1.635	1.687	1.753	1.833	1.940	2.089	2.300	2.654	3.412
0.4		1.645	1.708	1.784	1.881	2.009	2.186	2.439	2.865	3.800
0.6		1.663	1.739	1.836	1.954	2.106	2.314	2.619	3.125	4.250
0.8		1.684	1.781	1.898	2.037	2.217	2.460	2.809	3.394	4.704
1.0		1.711	1.829	1.968	2.127	2.335	2.605	3.003	3.665	5.127

Table 2(b) The phase angle, $\psi_V(\alpha,\beta,H)$, for delamination of a bilayer subjected to double transverse shear loads and $\beta = 0$. The uncertainties are ± 0.2° for $H \geq 0.2$.

	α	-0.8	-0.6	-0.4	-0.2	0	0.2	0.4	0.6	0.8
H										
0.0		see Table 3(b)								
0.2		+4.6°	+3.4°	+2.1°	+0.7°	-0.6°	-2.1°	-3.6°	-5.1°	-6.6°
0.4		+4.5°	+3.3°	+1.9°	+0.6°	-0.8°	-2.1°	-3.5°	-4.8°	-5.9°
0.6		+4.5°	+3.3°	+2.1°	+0.8°	-0.5°	-1.8°	-3.1°	-4.3°	-5.3°
0.8		+4.7°	+3.5°	+2.3°	+1.0°	-0.3°	-1.5°	-2.7°	-3.9°	-5.0°
1.0		+4.8°	+3.7°	+2.5°	+1.3°	0.0°	-1.3°	-2.4°	-3.6°	-4.9°

Table 3(a) The coefficient $f_{V_1}(\alpha,\beta,H)$ (with β = 0) for delamination of a bilayer subjected to a single transverse shear load on the arm 1. The uncertainties are ± 0.007 for $H \geq 0.2$ and ± 0.03 for H = 0.

	α	-0.8	-0.6	-0.4	-0.2	0	0.2	0.4	0.6	0.8
H										
0.0		1.64	1.69	1.76	1.84	1.94	2.09	2.29	2.61	3.28
0.2		1.607	1.628	1.662	1.715	1.791	1.902	2.075	2.380	3.055
0.4		1.531	1.507	1.510	1.545	1.618	1.729	1.908	2.214	2.851
0.6		1.413	1.354	1.351	1.386	1.458	1.573	1.746	2.023	2.518
0.8		1.282	1.206	1.206	1.247	1.323	1.434	1.590	1.812	2.137
1.0		1.150	1.077	1.088	1.133	1.207	1.306	1.438	1.607	1.787

Table 3(b) The phase angle, $\psi_{V_1}(\alpha,\beta,H)$ (with β = 0) for delamination of a bilayer subjected to single transverse shear load on arm 1. The uncertainties are ± 0.1° for $H \geq 0.2$ and ± 0.5° for H =0.

	α	-0.8	-0.6	-0.4	-0.2	0	0.2	0.4	0.6	0.8
H										
0.0		+5.0°	+4.0°	+3.0°	+2.0°	+0.7°	-0.5°	-1.7°	-3.1°	-4.8°
0.2		+4.3°	+2.6°	+0.8°	-1.2°	-3.5°	-6.0°	-8.7°	-11.7°	-15.1°
0.4		+3.2°	+0.6°	-2.0°	-4.6°	-7.4°	-10.0°	-12.6°	-15.2°	-17.9°
0.6		+1.6°	-1.9°	-4.9°	-7.6°	-10.5°	-12.8°	-15.0°	-17.1°	-19.1°
0.8		-0.5°	-4.6°	-7.7°	-10.2°	-13.0°	-14.9°	-16.7°	-18.3°	-19.8°
1.0		-3.0°	-7.5°	-10.5°	-12.7°	-15.1°	-16.3°	-17.7°	-19.0°	-20.2°

Figure captions

Figure 1 The general beam-like geometry subjected to axial loads and bending moments for which the interfacial fracture mechanics have been determined by Suo and Hutchinson (1990).

Figure 2 A schematic illustration of vectorial addition of stress-intensity factors (and square roots of energy-release rates).

Figure 3 The general geometry of a layered material subjected to axial loads, bending moments and transverse shear loads.

Figure 4 **(a)** A beam-like geometry subjected to double transverse shear loads and double opposing bending moments. **(b)** A beam-like geometry subjected to a single transverse shear load and an opposing bending moment.

Figure 5 Comparison between the analytical results (curves) and finite-element results (data points) for a double-cantilever beam with $H = 1$ and different values of α. Plots are shown for **(a)** non-dimensional energy-release rate, and **(b)** phase angle.

Figure 6 Comparison between the analytical results (curves) and finite-element results (data points) for a thin film ($H = 0$) loaded by a transverse shear force on a thick substrate, for different values of α. Plots are shown for **(a)** the non-dimensional energy-release rate, and **(b)** the phase angle.

Figure 7 A comparison of the energy-release rate for a symmetrical double-cantilever beam undergoing large-scale deformation calculated

from finite-element results (closed circle) and from the analytical approach presented in this paper (closed diamond). The bending moments used in the analytical results were calculated from the deformations predicted by finite-element calculations.

Figure 8 Root rotation and shear on a section at the crack tip.

Figure 9 Plots of the coefficients for the root rotation angle as a function of α for $H = 1$ (open symbols) and $H = 0$ (closed symbols), and for $\beta = 0$.

Figure 10 A plot of the load *versus* displacement for a symmetrical double-cantilever beam calculated using a cohesive-zone model, for an initial crack length $a_o = 2h$.

Figure 11 An elastic foundation model for a double-cantilever beam used to analyze the effects of deformation between the centroidal axis of the arms and the mid-plane of the geometry, as proposed by Kanninen (1973, 1974).

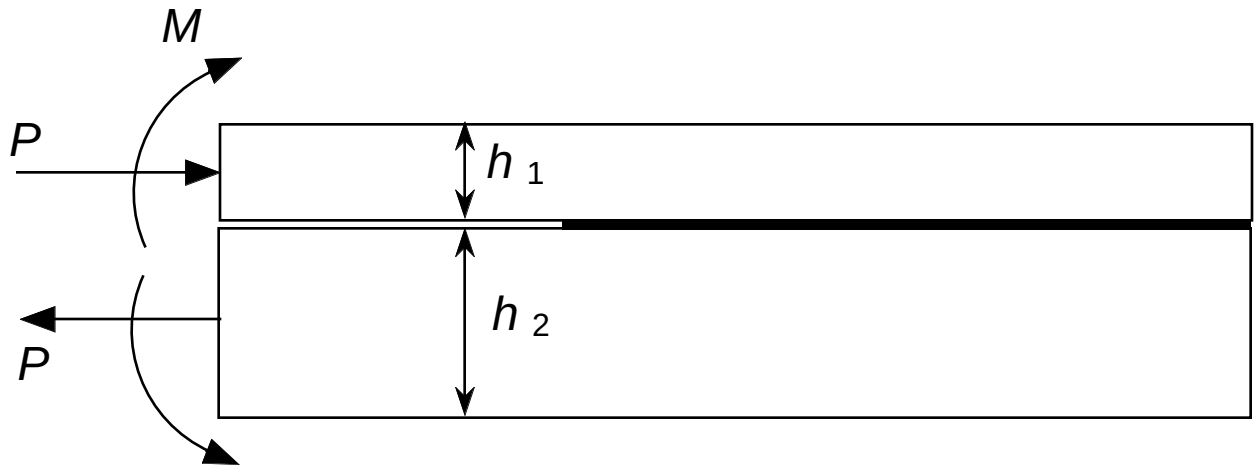

$$M^* = M + P\,(h_1 + h_2)\,/\,2$$

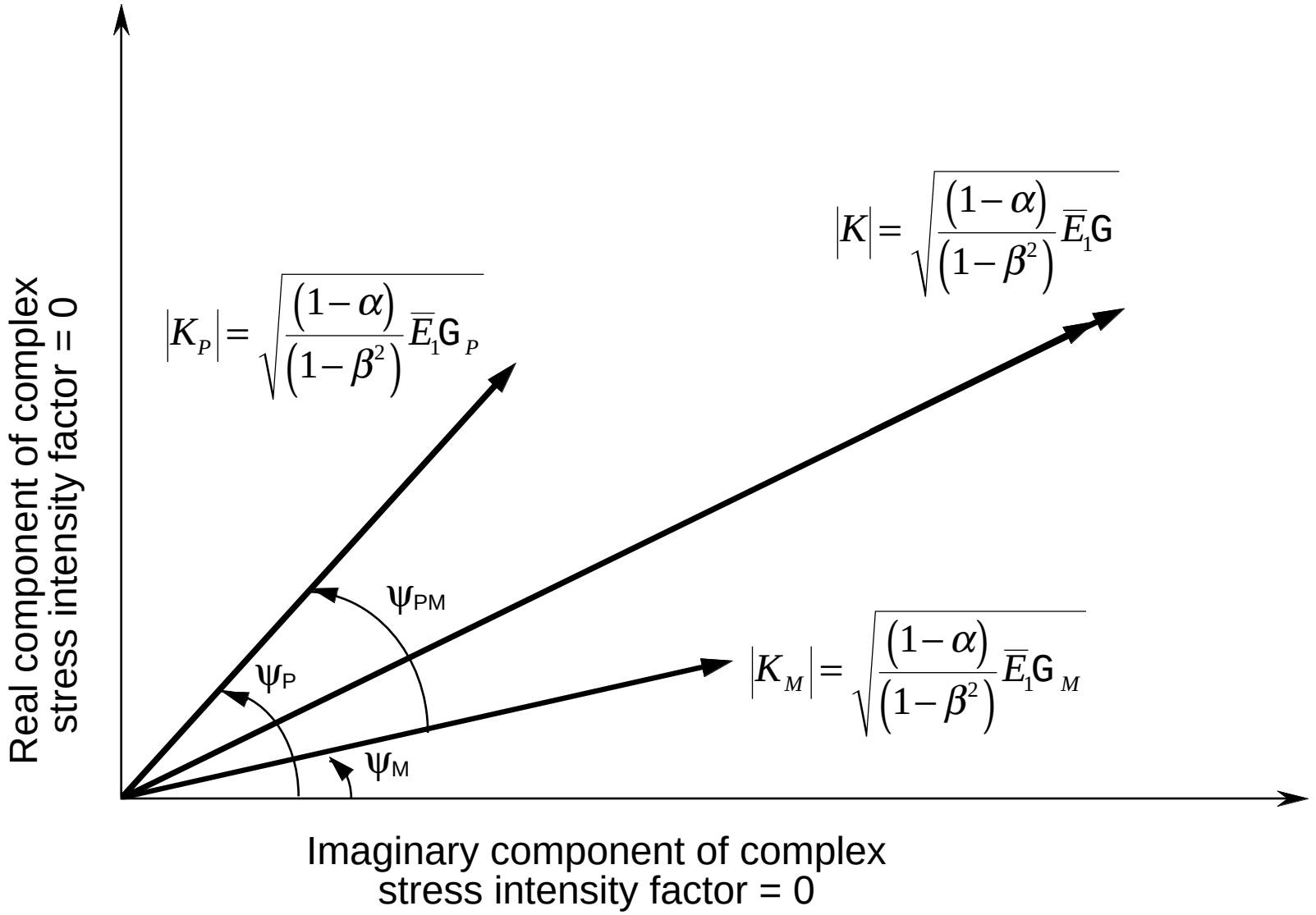
Real component of complex
stress intensity factor = 0
$|K_P| = \sqrt{\frac{(1-\alpha)}{(1-\beta^2)}\overline{E}_1 G_P}$
$|K| = \sqrt{\frac{(1-\alpha)}{(1-\beta^2)}\overline{E}_1 G}$
$|K_M| = \sqrt{\frac{(1-\alpha)}{(1-\beta^2)}\overline{E}_1 G_M}$
ψPM
ψP
ψM
Imaginary component of complex
stress intensity factor = 0

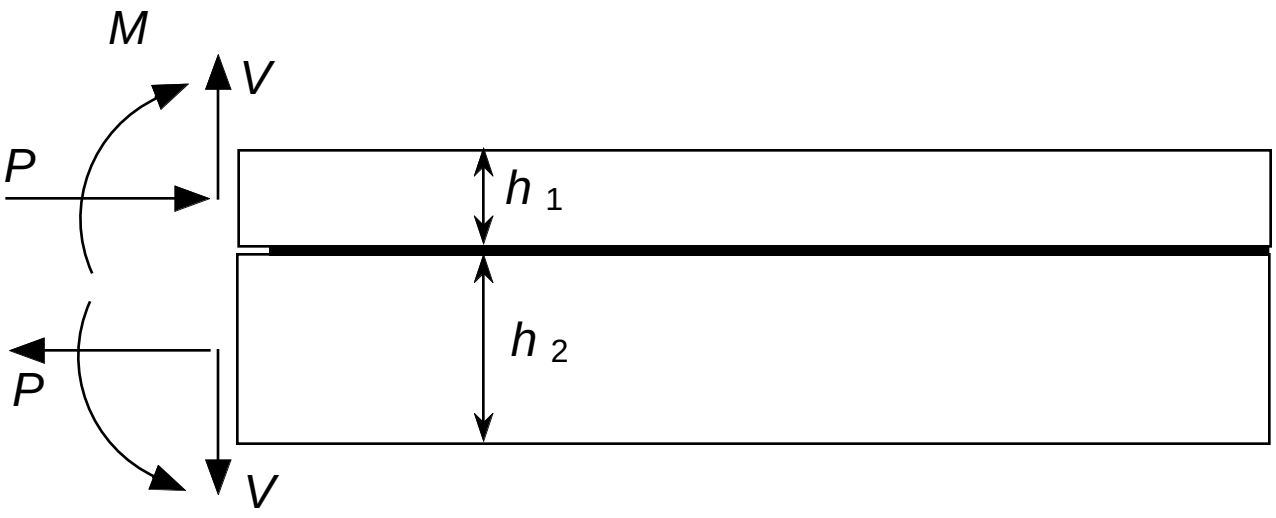

$$M^* = M + P\,(h_1 + h_2)\,/\,2$$

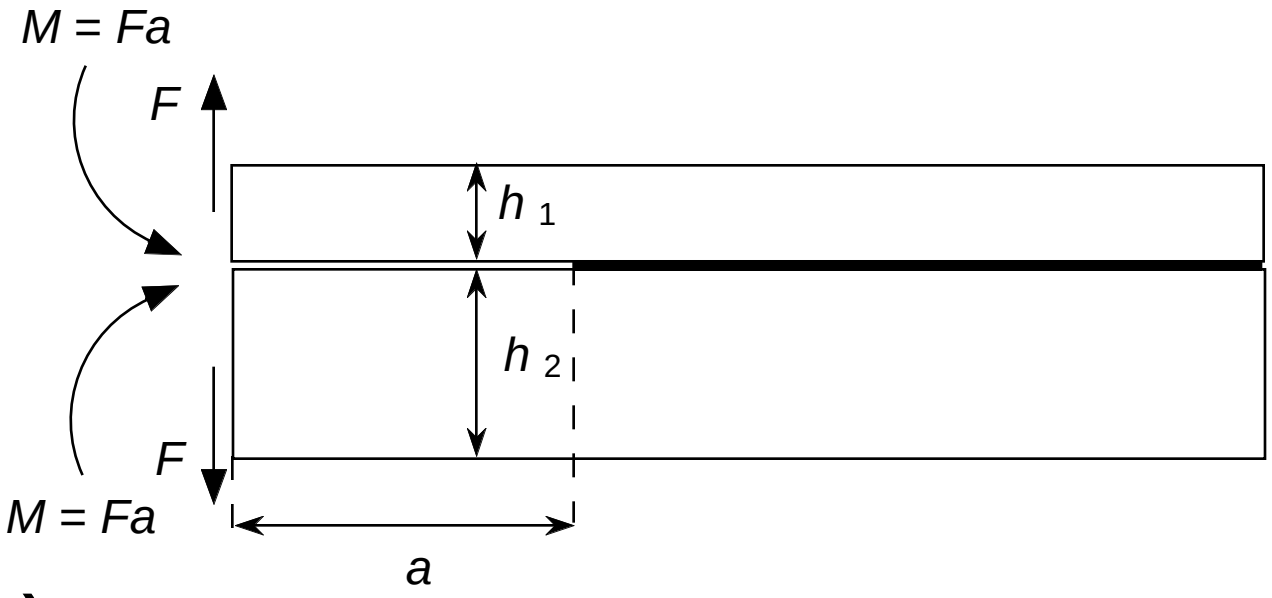

a)

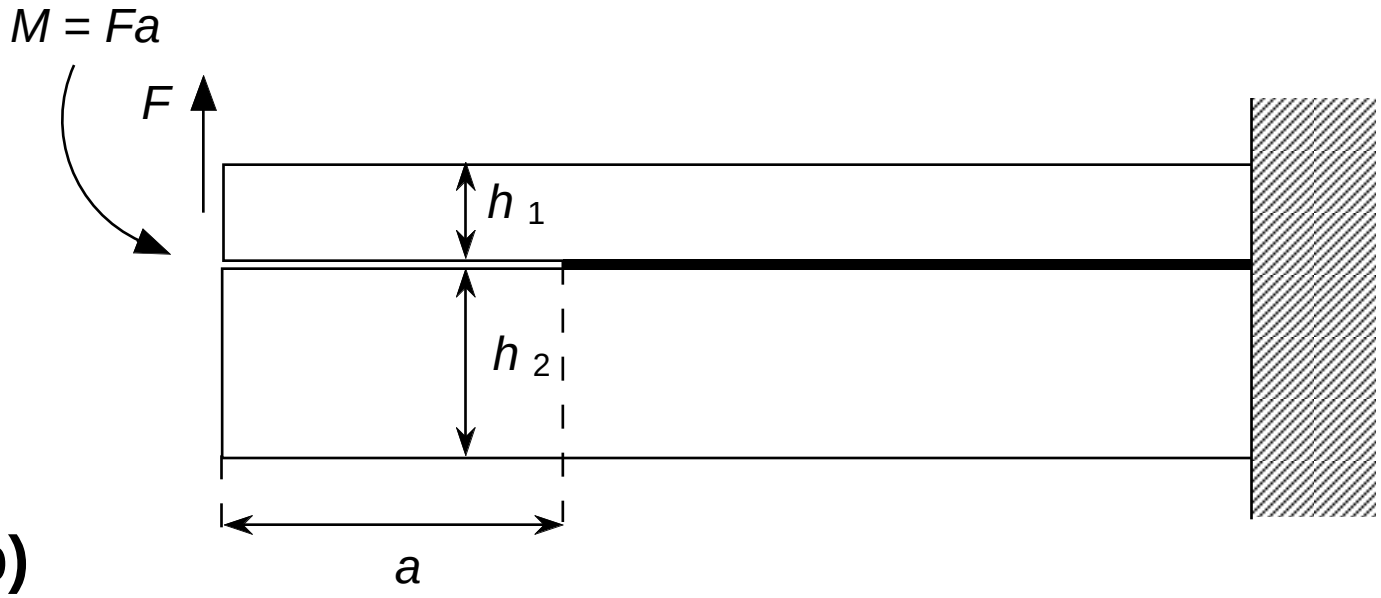

b)

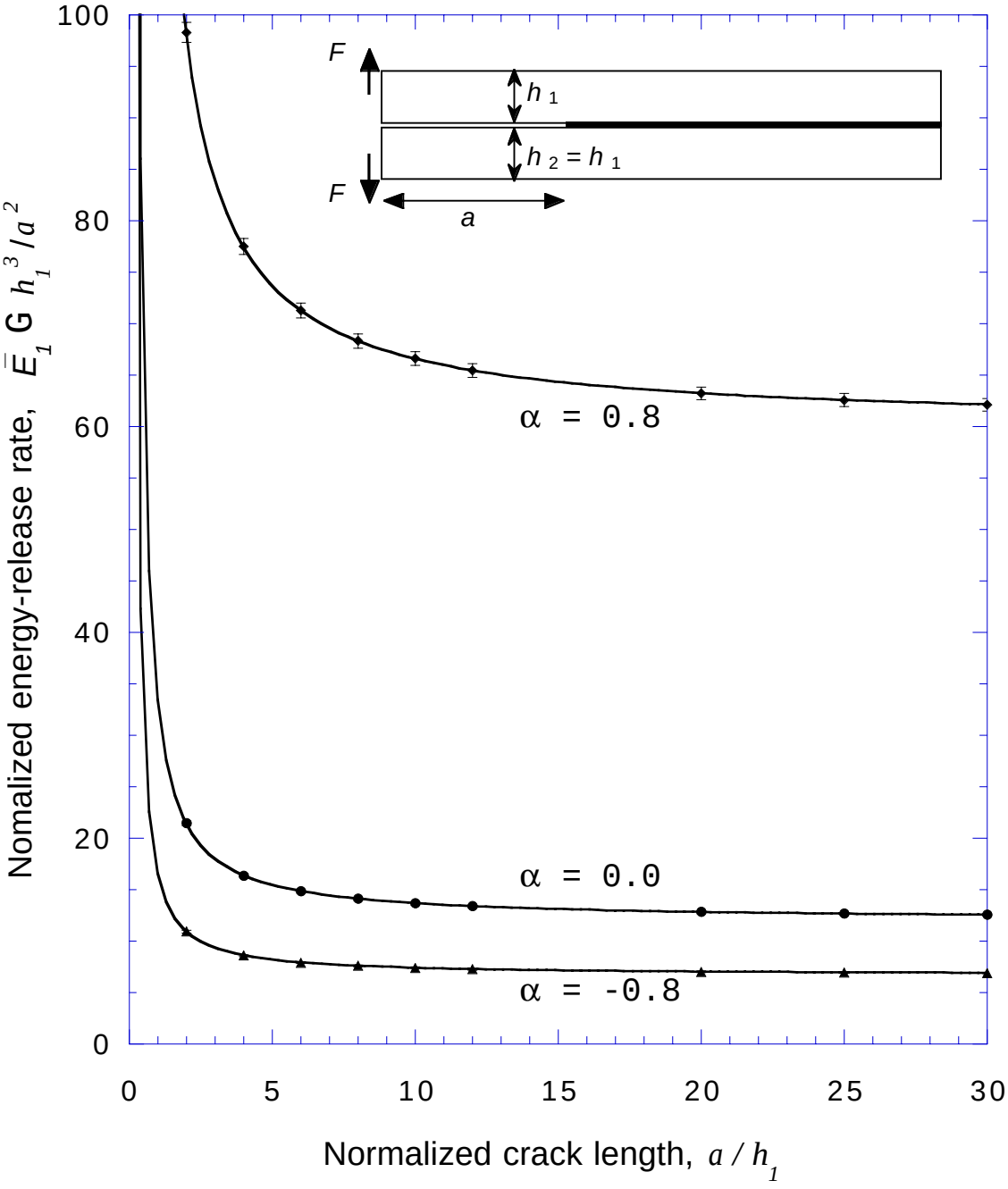
100
80
60
40
20
0
0
5
10
15
20
25
30
Nomalized energy-release rate, $\bar{E}_1 G h_1^3 / a^2$
Normalized crack length, a / h_1
F
h_1
$h_2 = h_1$
F
a
α = 0.8
α = 0.0
α = -0.8

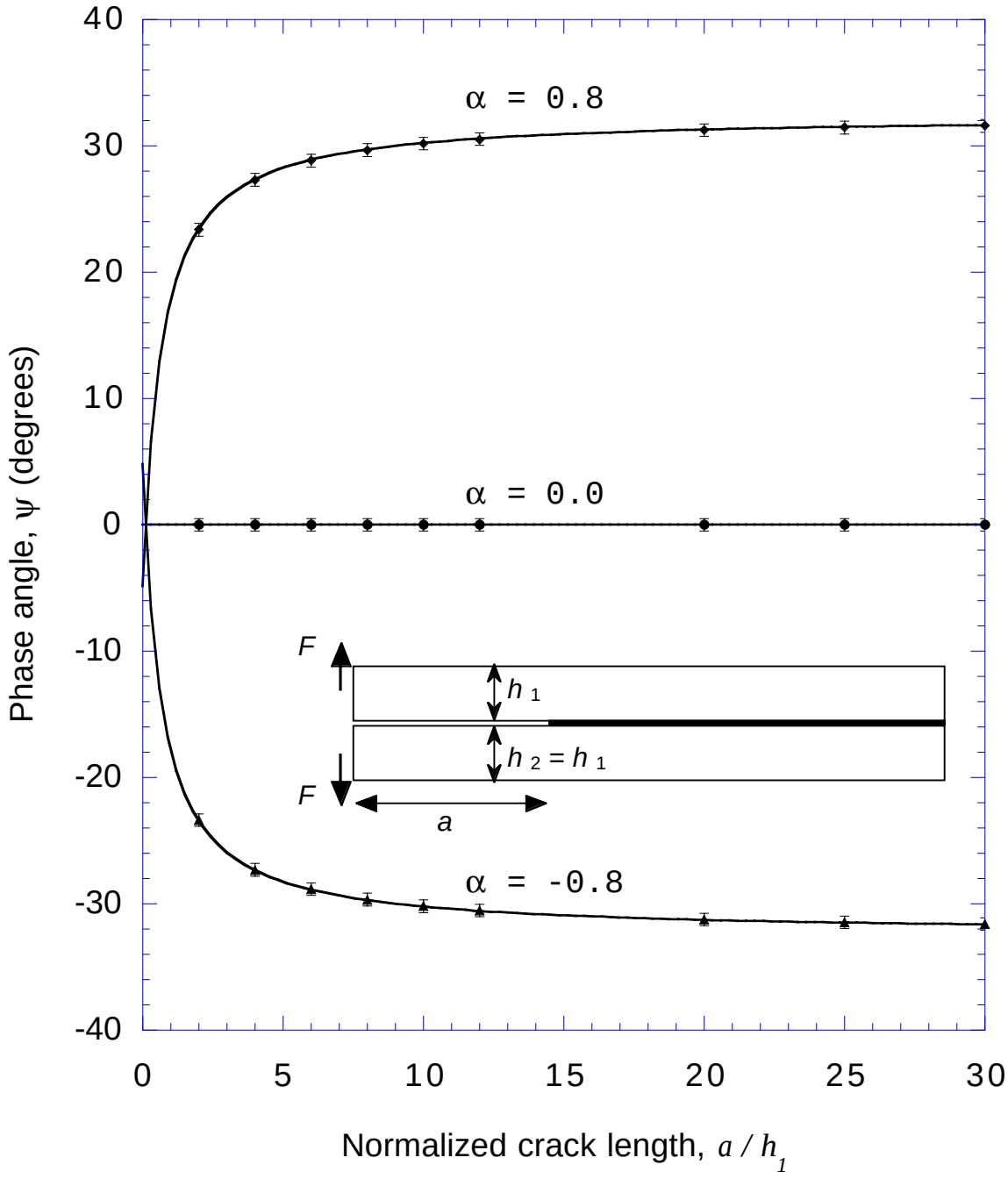
40
30
20
10
0
-10
-20
-30
-40
0
5
10
15
20
25
30
α = 0.8
α = 0.0
α = -0.8
Phase angle, ψ (degrees)
Normalized crack length, a / h1
F
h 1
h 2 = h 1
F
a

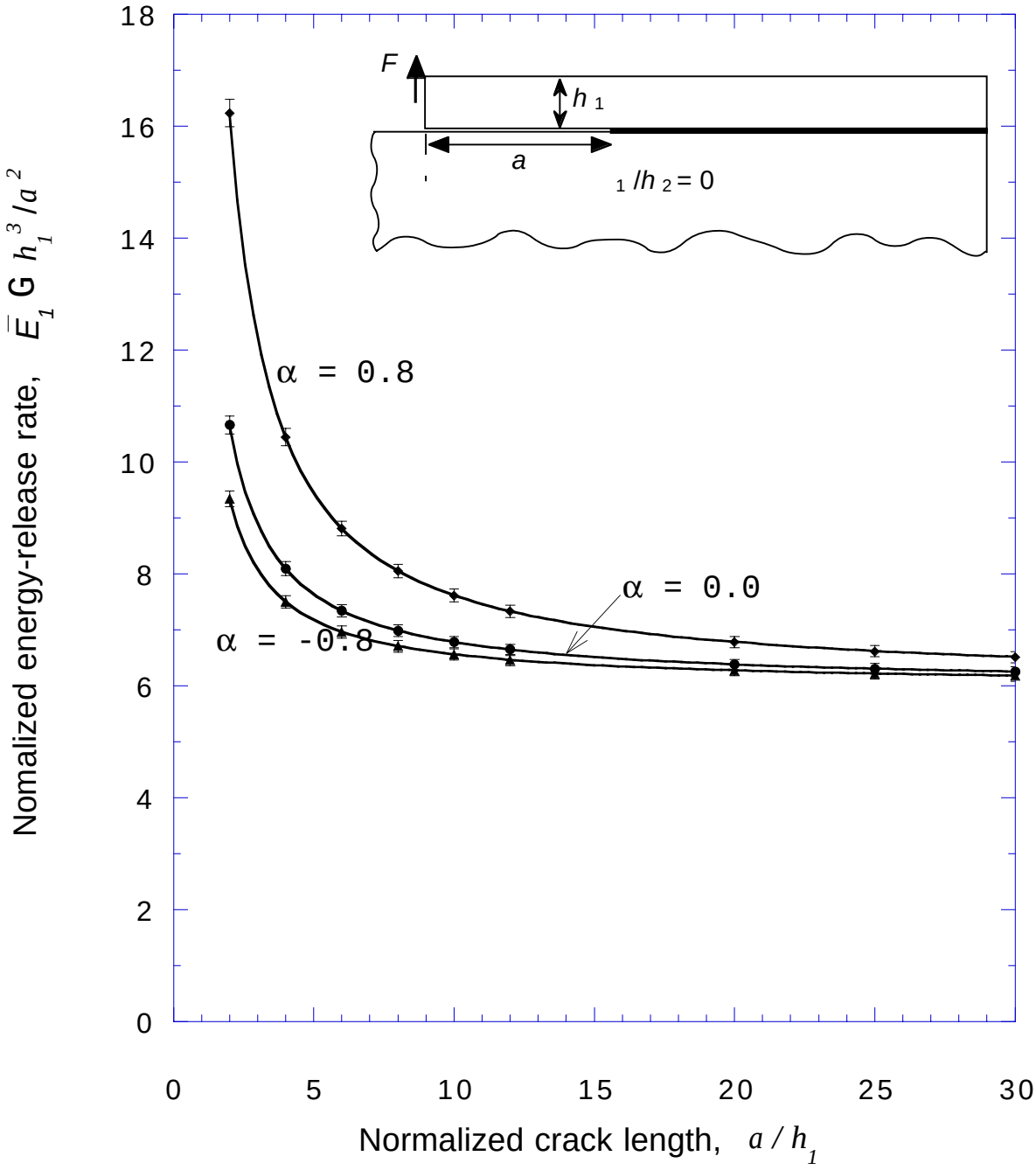
F
h 1
a
1 /h 2 = 0
α = 0.8
α = 0.0
α = -0.8
Nomalized energy-release rate, $\bar{E}_1 G h_1^3 / a^2$
Normalized crack length, a / h_1
0
2
4
6
8
10
12
14
16
18
0
5
10
15
20
25
30

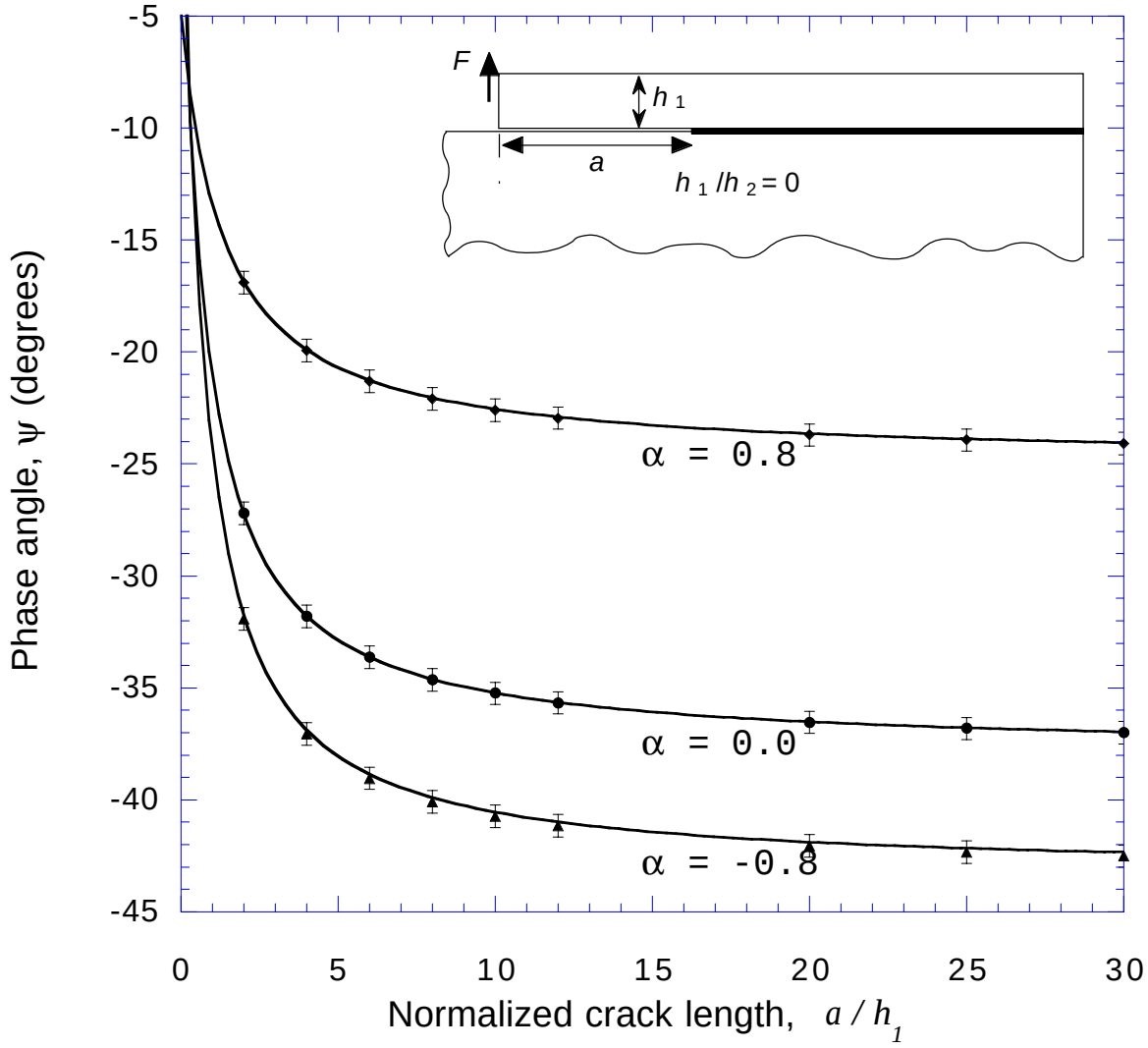
-5
-10
-15
-20
-25
-30
-35
-40
-45
0
5
10
15
20
25
30
Phase angle, ψ (degrees)
Normalized crack length, a / h1
F
h 1
a
h 1 /h 2 = 0
α = 0.8
α = 0.0
α = -0.8

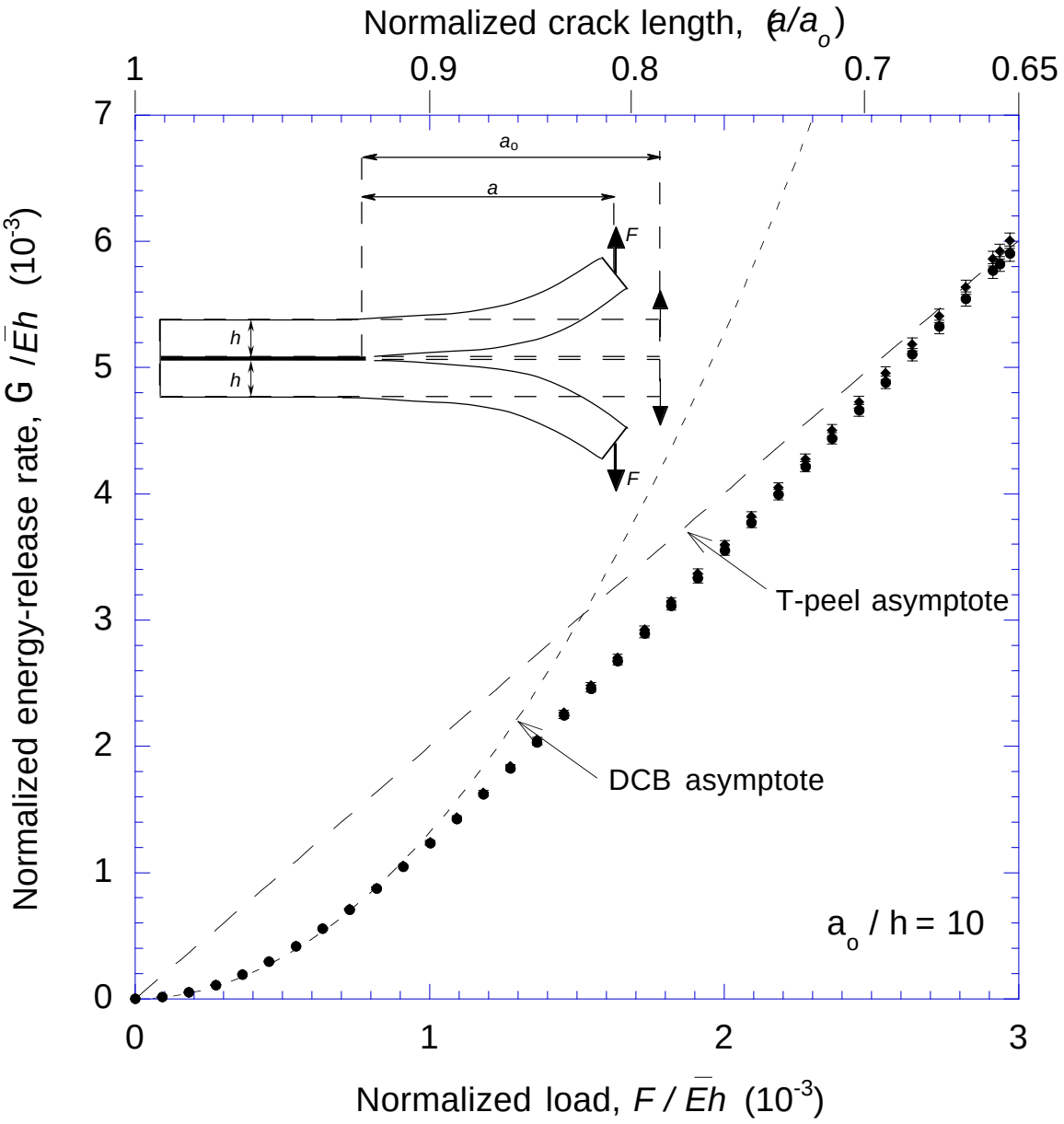
Normalized crack length, (a/a_o)
1
0.9
0.8
0.7
0.65
Normalized energy-release rate, $G/\bar{E}h$ (10^{-3})
7
6
5
4
3
2
1
0
a_o
a
F
h
h
F
T-peel asymptote
DCB asymptote
a_o / h = 10
0
1
2
3
Normalized load, $F/\bar{E}h$ (10^{-3})

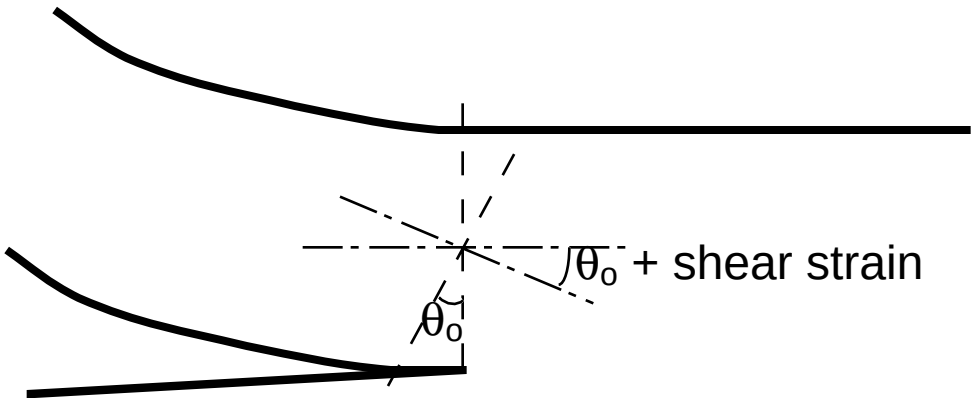
θo + shear strain
θo

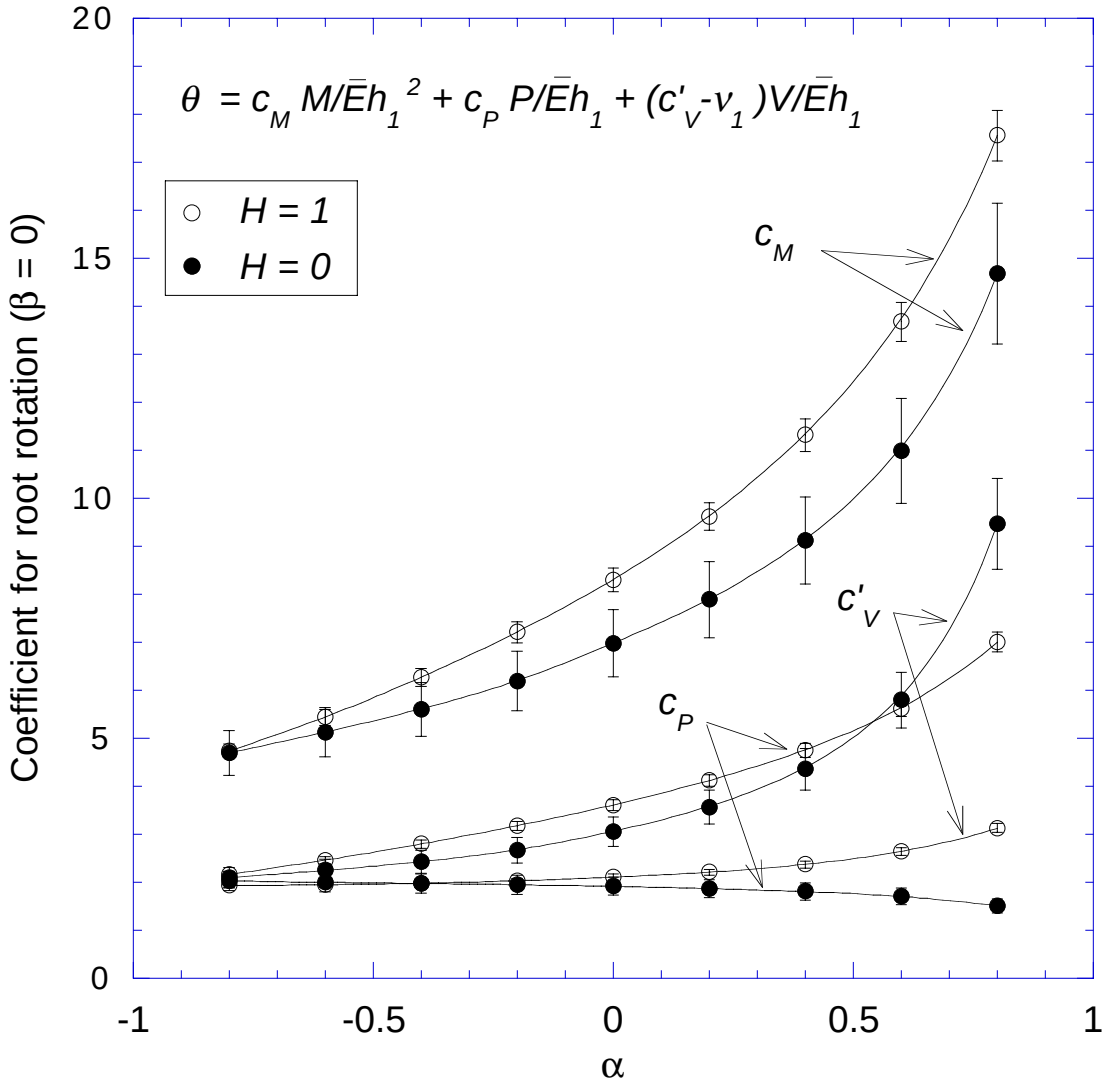
θ = c_M M/Ēh_1^2 + c_P P/Ēh_1 + (c'_V-ν_1)V/Ēh_1
H = 1
H = 0
c_M
c'_V
c_P
Coefficient for root rotation (β = 0)
α
20
15
10
5
0
-1
-0.5
0
0.5
1

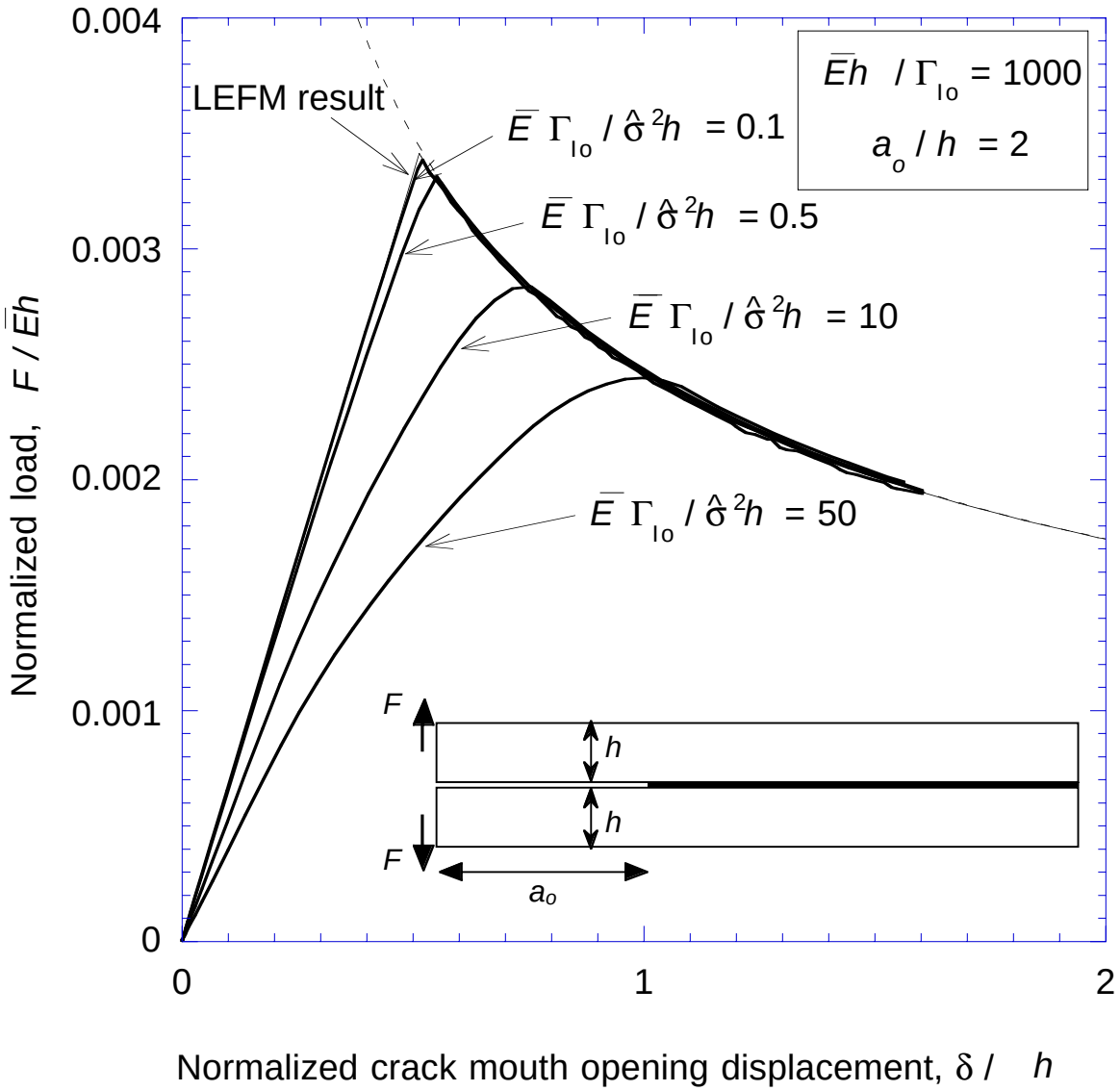
0.004
0.003
0.002
0.001
0
0
1
2
Normalized load, $F / \bar{E}h$
Normalized crack mouth opening displacement, δ / h
LEFM result
$\bar{E}\,\Gamma_{Io} / \hat{\sigma}^2 h = 0.1$
$\bar{E}\,\Gamma_{Io} / \hat{\sigma}^2 h = 0.5$
$\bar{E}\,\Gamma_{Io} / \hat{\sigma}^2 h = 10$
$\bar{E}\,\Gamma_{Io} / \hat{\sigma}^2 h = 50$
$\bar{E}h / \Gamma_{Io} = 1000$
$a_o / h = 2$
F
h
h
F
a_o

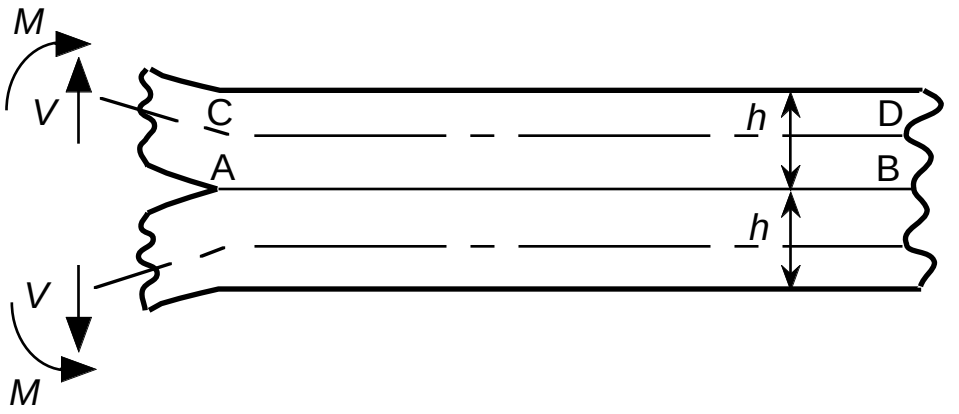
M
V
C
A
h
D
B
h
V
M

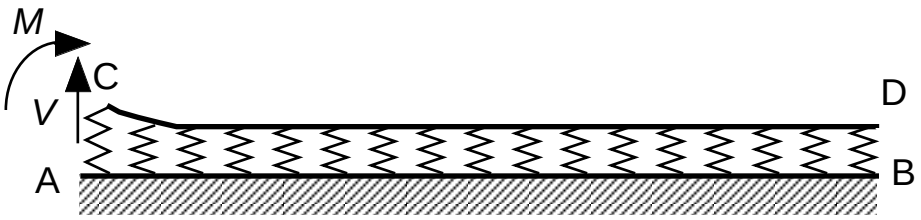
M
C
V
D
A
B